ISSN: 0067-2904

Evaluation of the Properties of Magnetite (Fe_3O_4) Nanoparticles Prepared by the Green Method *U*sing *Phoenix dactylifera* Extract

Zainab J. Shanan*, Huda M.J. Ali, Nisreen Kh. Abdalameer
Department of Physics, College of science for Women, University of Baghdad, Baghdad, Iraq

Received: 6/8/2022 Accepted: 19/11/2023 Published: 30/12/2024

Abstract

Iron oxide (Fe_3O_4) nanoparticles were synthesized via an eco-friendly green approach by adding *Phoenix dactylifera* extract to the aqueous solution of ferric chloride. The effect of annealing temperature (Ta) (100-150) °C on particle size was studied. X-ray diffraction (XRD), UV-visible spectroscopy, atomic force microscopy (AFM), and field emission scanning electron microscopy (FESEM) were used to evaluate the produced nanoparticles. According to XRD spectra, the crystallite size of the samples was determined using the Scherrer formula. AFM and FE-SEM were used to determine surface morphology. A UV-Vis optical spectroscopic examination was carried out to determine the band gap energy of the iron oxide nanoparticles. It was found that with the increased temperature from 100 to 150 ºC, the band gap energy of the produced Fe_3O_4 NPs decreased. The size of the produced particles increased with increasing temperature, as evidenced by AFM and XRD spectra.

Keywords: Iron oxide nanoparticles; *Phoenix dactylifera* extract; green approach; atomic force microscopy; scan electron microscopy.

تقييم خواص جسيمات المغنيت (Fe_2O_3) النانوية المحضرة بالطريقة الخضراء بأستخدام *Phoenix dactylifera*

زينب جاسم شنان*, هدى محمد جعفر علي, نسرين خليل عبد الامير
قسم الفيزياء, كلية العلوم للبنات, جامعة بغداد, بغداد, العراق

الخلاصة

تم تصنيع جسيمات أوكسيد الحديد (Fe_3O_4) النانوية بطريقة خضراء صديقة للبيئة عن طريق إضافة مستخلص Phoenix dactylifera إلى المحلول المائي لكلوريد الحديديكز تم دراسة تأثير درجة الحرارة (100–150) درجة مئوية على حجم الجسيمات. استخدم حيود الأشعة السينية (XRD)، والتحليل الطيفي المرئي للأشعة فوق البنفسجية ، والفحص المجهري للقوة الذرية (AFM)، والفحص المجهري الإلكتروني (FESEM) لتقييم الجسيمات النانوية الناتجة. وفقًا لأطياف XRD ، تم حساب الحجم البلوري للعينات باستخدام صيغة Scherrer. وتم استخدام AFM و FE–SEM لتحديد مورفولوجيا السطح وحجم الجسيمات. بينما تم إجراء الفحص الطيفي البصري للأشعة المرئية وفوق البنفسجية لتحديد فجوة الطاقة لجسيمات أوكسيد الحديد النانوية ، حيث تم اكتشاف أنه مع زيادة درجة الحرارة من 100 إلى 150 درجة مئوية ، تقل فجوة

*Email: zainabjs_phys@csw.uobaghdad.edu.iq

الطاقة لجسيمات Fe3O4 النانوية الناتجة. يزداد حجم الجسيمات الناتجة مع زيادة درجة الحرارة ، كما يتضح من أطياف AFM و XRD.

1. Introduction

Nanotechnology is the manipulation of matter using chemical and/or physical methods to create nanosized materials with specified qualities that can be employed in specific applications [1]. These materials have unique optical, thermal, electrical, chemical, and physical qualities that make them useful in medicine, chemistry, agriculture, information and communication, heavy industry, and consumer products [2][3]. Traditional methods of nanoparticle synthesis, such as attrition and pyrolysis, have limitations such as faulty surface formation, limited production rate, and expensive manufacturing costs [4]. In the chemical synthesis processes (e.g., chemical reduction, sol-gel technique, etc.), toxic chemicals are used, in addition potentially harmful byproducts are produced and pollutants derived from precursor substances are emitted [4]. Biological synthesis has gotten a lot of interest because it is a unique strategy and an alternative to physical and chemical procedures [5]. Biological synthesis processes have several distinct advantages over traditional physical and chemical methods, where toxic chemicals are not employed, making this a clean and environmentally friendly approach [6]. The phytochemicals reduce the raw materials to metal nanoparticles in the bottom-up process. Alkaloids, phenolic chemicals, terpenoids, and coenzymes are some of the reducing agents used in nanoparticle formation. Bioactive chemicals can potentially be a capping and stabilizing agent [6][7]. Simple prokaryotic bacteria and eukaryotes like fungi and plants are used in the biosynthesis process. In contrast to microorganisms, bio-green synthesis has a significant advantage because plant-mediated synthesis is a one-step process. However, microbes may lose their ability to produce nanoparticles over time as a result of mutation; also, the procedure is exceedingly arduous and time-consuming [7]. Nanoscale materials with magnetic characteristics have gained scientists' interest, and they have a wide range of applications [8][9]. Researchers in various fields, including biotechnology, biomedicine, magnetic fluids, magnetic resonance imaging, and environmental remediation, are interested in magnetic nanoparticles [10]. When a particle size is less than a nanometer, its magnetic properties are modified, causing new phenomena including magnetic resistance, superparamagnetism, strong coercively, a drop in Curie/Neel temperature, and low or high magnetization [10-12]. Iron oxide, also known as wüstite (FeO), hematite (□□□Fe_2O_3), maghemite (□□ Fe_2O_3), and magnetite (Fe_3O_4), are transitional metal oxides that crystallize in a variety of stoichiometric and crystalline structures [13-15].

In this study, the green approach was used to synthesize iron and iron oxide nanostructures in liquids. The effect of temperature on several physical properties, such as structural, morphological, and optical qualities of the manufactured material, was evaluated.

2. Experimental work

2.1 Materials

Without further purification, iron (III) chloride / ferric chloride ($FeCl_3$) was used. Throughout this study, deionized water (DI) was used. 0.4055gm of the solid $FeCl_3$ was dissolved in 90 ml DI water to make a $FeCl_3$ (1mM) solution. Phoenix dactylifera (date palm) is a relatively inexpensive reducing and stabilizing agent.

2.2 Preparation of Phoenix dactylifera extract

To make the extract, *Phoenix dactylifera* was washed thoroughly to remove any adhered soil and dust. 20g of *Phoenix dactylifera* was mixed with 200 ml of deionized water. The

solution was heated for 1 hour at about 50°C on a magnetic stirrer, then filtered through filter paper to separate the liquid. For future studies, the extract was kept at 4℃.

2.3 Synthesis of Iron Oxide

The produced *Phoenix dactylifera* extract was utilized to reduce and cap the Fe ions in the conventional manufacture of iron oxide. 150 mL of the prepared *Phoenix dactylifera* extract was gradually added to the $FeCl_3$ aqueous solution with constant stirring for two hours at 70 °C. Within 3 minutes of introducing the *Phoenix dactylifera* extract to the $FeCl_3$ solution, visible color changes were seen; the yellow aqueous color of the $FeCl_3$ solution turned greenish-black, indicating the formation of iron oxide nanoparticles. The solution was centrifuged for 40 min at 4000 rpm to separate the produced nanoparticles. These nanoparticles were further centrifuged three times for five minutes with deionized water before being dried in an oven for one hour and heated in the furnace for two hours at 100 and 150°C. The resulting material was then cooled, and ground the produced powder was collected for analysis.

3. Results and Discussions

3.1 X-Ray Diffraction Analysis (XRD)

XRD measurement was used to identify the crystalline structure of the two powders. The XRD patterns of these two powder samples are shown in Figure (1). The position and relative intensity of the main peaks match well those from the JCPDS card (19–0629) for Fe_3O_4, confirming that the product is iron oxide(Fe_3O_4) [16]. The broadening of the absorption spectra can be attributed to the quantum confinement phenomenon exhibited by the nanoparticles [17]. The appearance of extra peaks at orientation (300) and (422) for the sample annealed at 150 ^oC is due to increased crystallization growth can be inferred from the XRD peak intensity as shown in Figure (1). It was also noticed that the intensity of the peak and the size of the crystal increased with the increase in temperature.

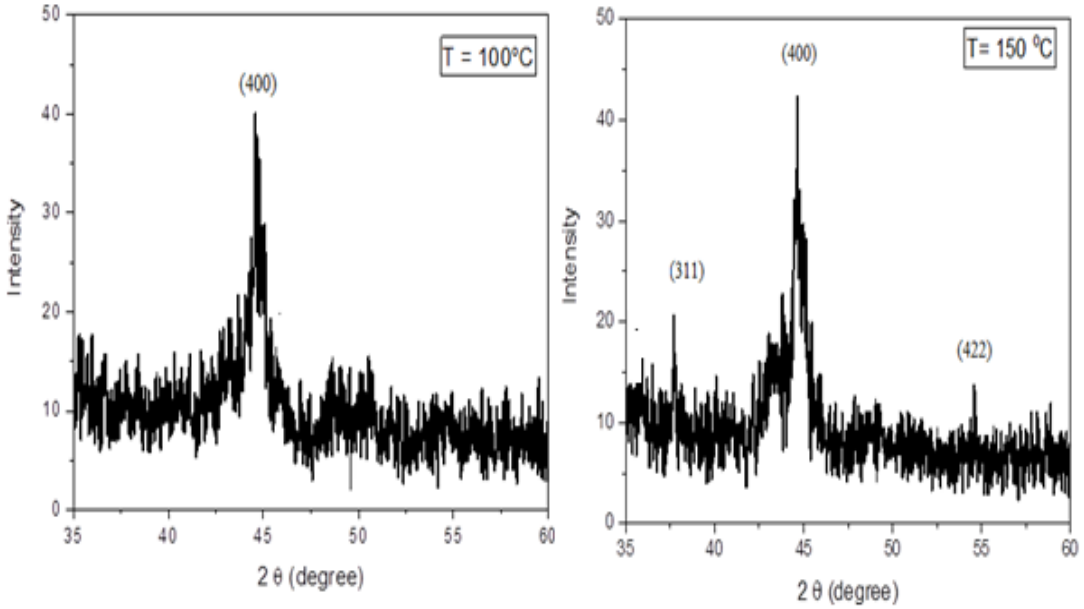

Figure 1: The XRD patterns of as-prepared Fe_3O_4 NPs at two temperatures**.**

The XRD patterns of the two samples identified the cubic structure of Fe_3O_4, revealing that the iron oxide was of a relatively pure phase. The crystallite size (D) was calculated using the Scherrer equation [18]:

$$D = \frac{0.9\lambda}{\beta \cos\theta} \quad (1)$$

Where: λ is the wavelength of the incident X-ray (1.5406 ˚A), θ is the degree of the diffraction peak, and β is the full width at half maximum (FWHM) of the XRD peak appearing at the diffraction angle θ. Table (1) contains the structural properties parameters of Fe_3O_4 NPs as deduced from the XRD study.

Microstrain (ε) is caused by lattice mismatch, which changes according to deposition conditions and is determined using the formula [19]:

$$\varepsilon = \frac{\beta \cos\theta}{4} \quad (2)$$

To have information on the number of imperfections in the samples, the dislocation density (□) was calculated using the formula [20]:

$$\delta = \frac{1}{(D)^2} \quad (3)$$

It was observed that the dislocation density decreased with the increase in the crystallite size. Similarly, the microstrain increased with the decrease in crystallite size. The negative value of the microstrain revealed the compressive strain of the Fe_3O_4 NPs. These results are shown in Table 1.

Table 1: the parameters of structural properties of Fe_3O_4 NPs at two annealing temperatures.

T (°C)	2□ (deg.)	□ (rad)	d Exp. (°A)	d Sta. (°A)	a Exp. (°A)	a Sta. (°A)	hkl	Crystallite Size (nm)	□ x10^{-2} lines/m^4	□ x10^{15} lines/m^2
100	44.61	0.44	2.029	2.09	8.116	8.39	(400)	17.02	-3.98	3.45
	37.70	-	-	-	-	-	(311)	-	-	-
150	44.65	0.31	2.027	2.09	8.111	8.39	(400)	24.00	-3.31	1.73
	54.6	-	-	-	-	-	(422)	-	-	-

3.2 Surface Topological Analysis

Microscopic surface structure information is gathered using atomic force microscopy, and topography is displayed as surface topography (AFM). This method makes use of digital photographs to allow for quantitative evaluations of surface qualities such as root squared roughness, Rq, or mean roughness, Ra, as well as image analysis from several angles, including 3D modeling [21]. Two and three-dimensional AFM images of the two samples and height distributions are shown in Figures 2 and 3. The images showed that the sample subjected to annealing at 100°C exhibited smaller clusters with an average mean diameter of 61.80 nm, as well as a higher presence of surface aggregates compared to the sample annealed at 150°C, which had an average grain size of 87.15 nm in diameter. The increase in the annealing temperature increased the crystal size. It can be noted that the average diameter of the nanoparticles measured by the AFM was larger than those obtained by the XRD. This could be explained by the fact that the analysis is statistical, and that certain "particles" agglomerated leading to the formation of larger particles that are more conspicuous and possess greater height.

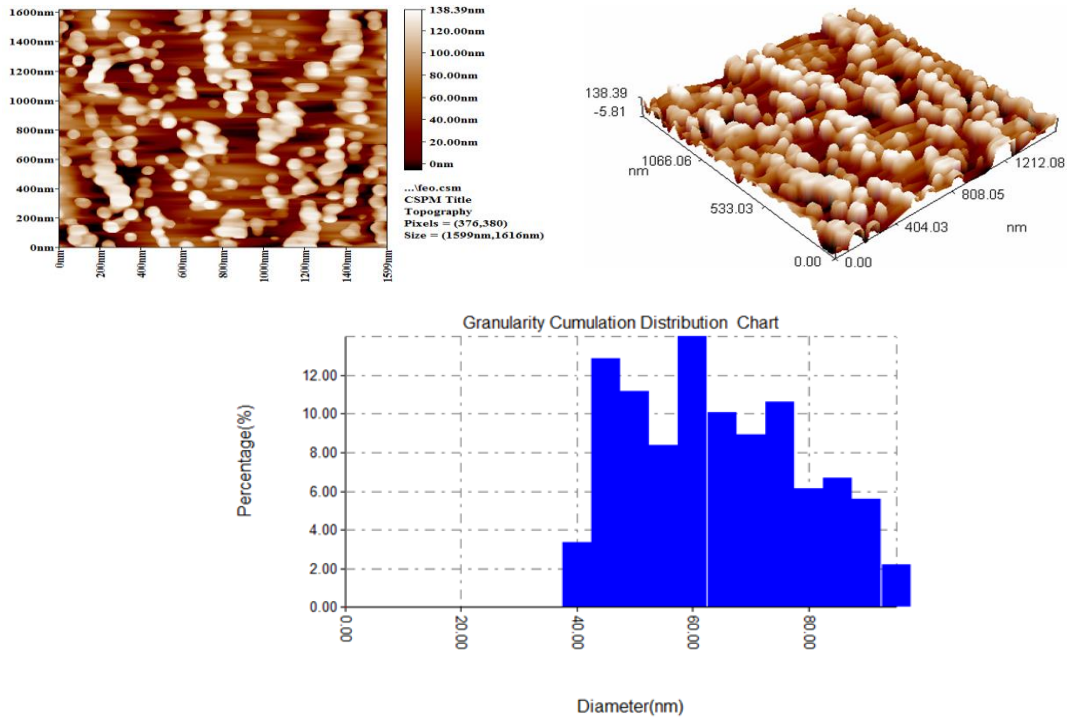

Figure 2: 2D and 3D AFM images of Fe_3O_4 NPs and height distribution at Ta= 100ºC.

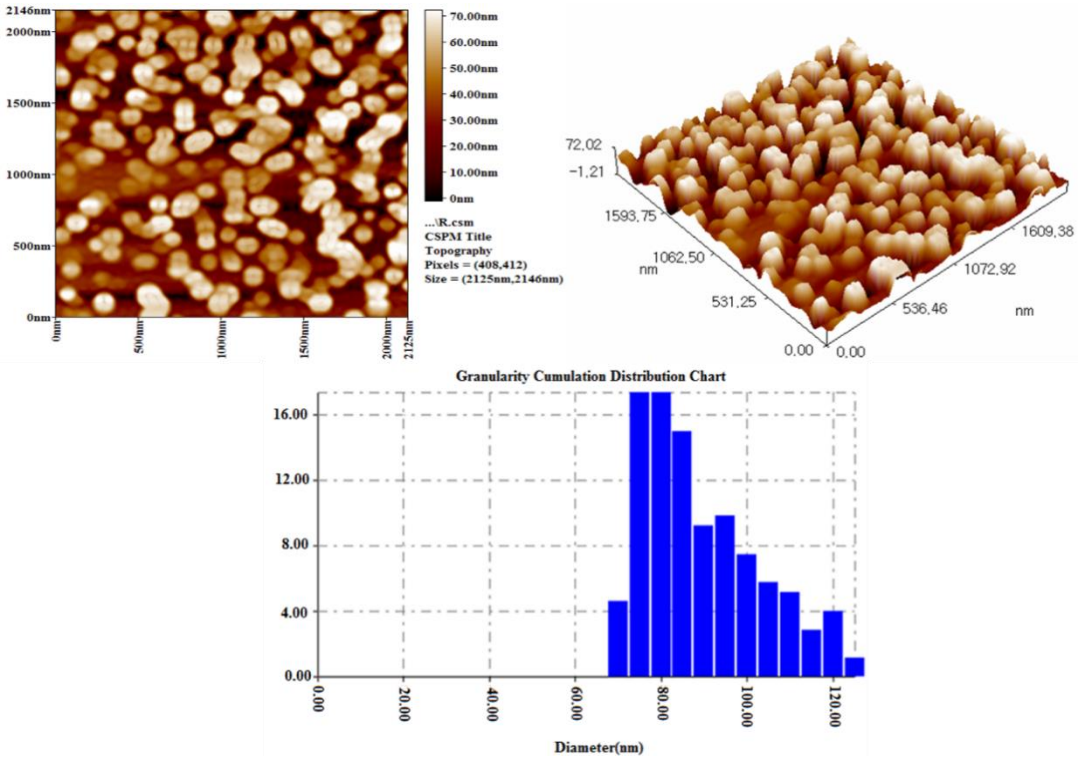

Figure 3: 2D and 3D AFM images of Fe_3O_4 NPs and height distribution at Ta= 150ºC.

3.3 Surface Morphological Analysis

The surface shape and particle size of the prepared Fe_2O_3 NPs were studied by FE-SEM at the two annealing temperatures (100 and 150)ºC, as shown in Figure 4. Since the specific surface area (surface-to-volume ratio) is significant, aggregation of particles occurred as expected. From the images, it can be seen that most of the nanoparticles began to merge when the temperature was increased from 100ºC to 150ºC, and agglomerated to take on an almost

spherical shape. The particle size diameters ranged from 26.05 to 63.27 nm for Ta= 100ºC, while it ranged from 40.94 to 111.7 nm for Ta= 150°C. The increase in particle size as temperature increases is attributed to increased particle growth and, as a result, improved crystallization of the material. The X-ray diffraction and atomic force microscope measurements support these findings.

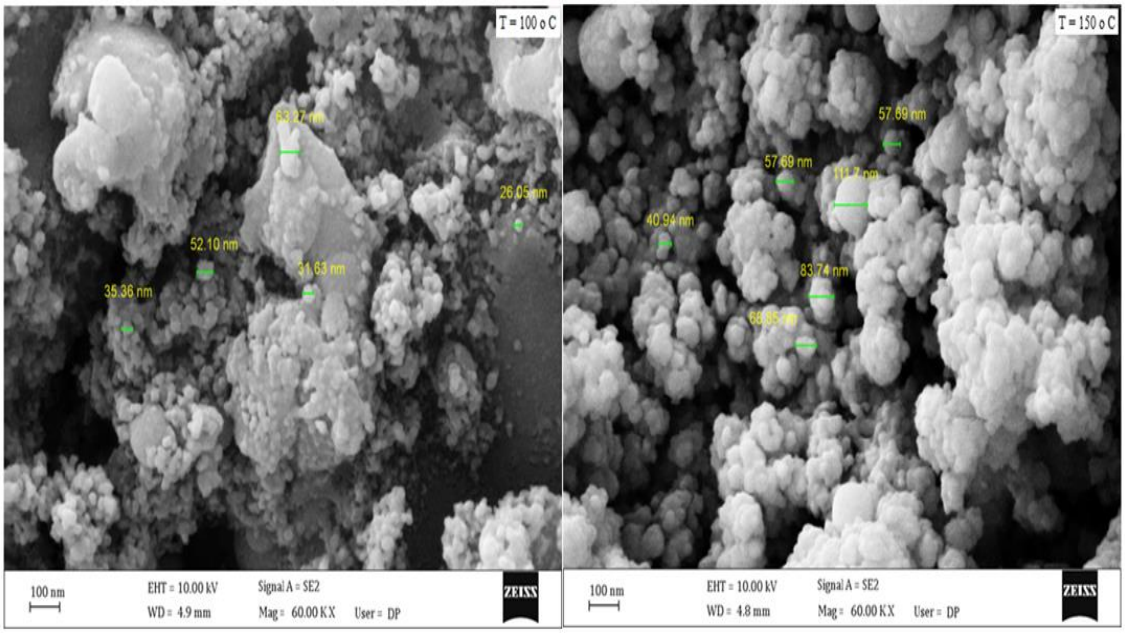

Figure 4: Field emission scanning electron microscopy images for the prepared Fe_3O_4 NPs at both annealing temperatures.

Figure 5 illustrates the results of the energy-dispersive X-ray spectroscopy (EDX) for Fe_2O_3 NPs at the two annealing temperatures. There were distinct peaks corresponding to Fe at (0.6-0.8) keV, (6.1-6.5) keV and O at (0.2–0.4) keV. Peaks for C, Cl, and P were also noticed.

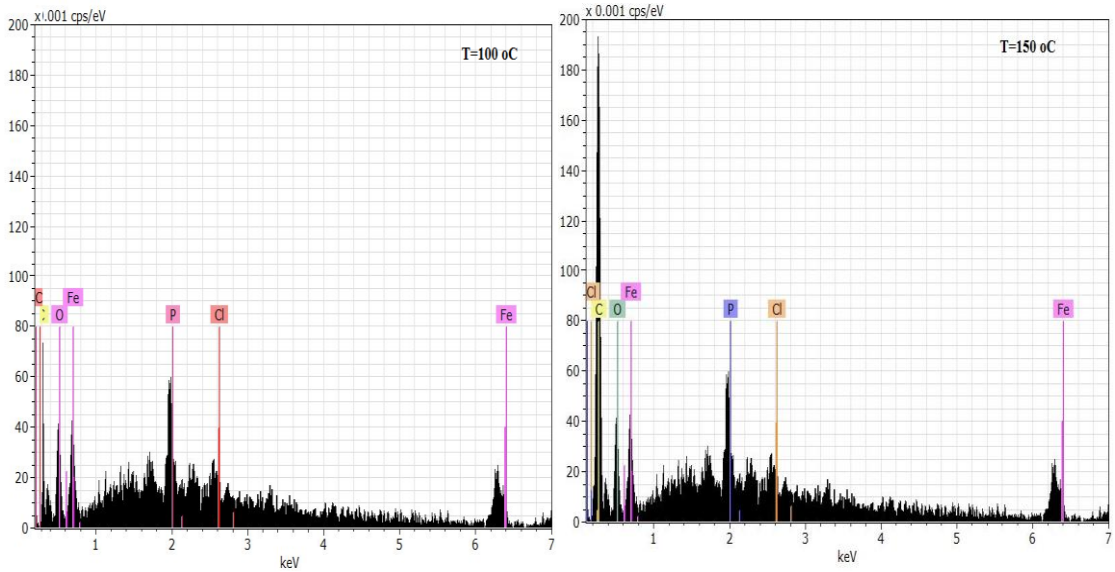

Figure 5: EDX analysis for the prepared Fe_3O_4 NPs at both annealing temperatures**.**

3.4 Optical absorption analysis

One of the most essential parameters for evaluating the optical activity of Fe_3O_4 nanoparticles is their optical property. The phenomenon of UV/Visible absorption entails the absorption of radiant energy by the outer electrons of atoms or molecules, resulting in their transfer to higher energy levels. The spectrum acquired from the optical absorption can be studied to determine the band gap energy of semiconductor nanoparticles. The absorption spectrum of iron oxide NP solution as-grown at the two annealing temperatures (100 and 150)^o C and prepared by the green method is presented in Figure 6. The band gap energy(Eg) was calculated using the equation:

$$E_g = hc/\lambda_{cut} \quad (4)$$

Where: *h* is Plank's constant, and λ_{cut} is the cut-off wavelength of 380 nm and 420 nm for Ta=100^o C, and 150^o C, respectively.

The values of band gap energy for Fe_3O_4 NPs at Ta= (100^{o}C) was 3.26 eV, whereas at Ta= (150^{o}C), it was decrease to 2.95 eV at the specified cut-off wavelengths; which are blue-shifted from the value of the bulk Fe_3O_4 (Eg = 2.4 eV); the reduction of the band gap energy can be attributed to the increased crystallization and thus increased grain size. The quantum confinement effect was indicated by the increase of the band gap energies of Fe_3O_4 nanoparticles owing to the reduction of the structure size.

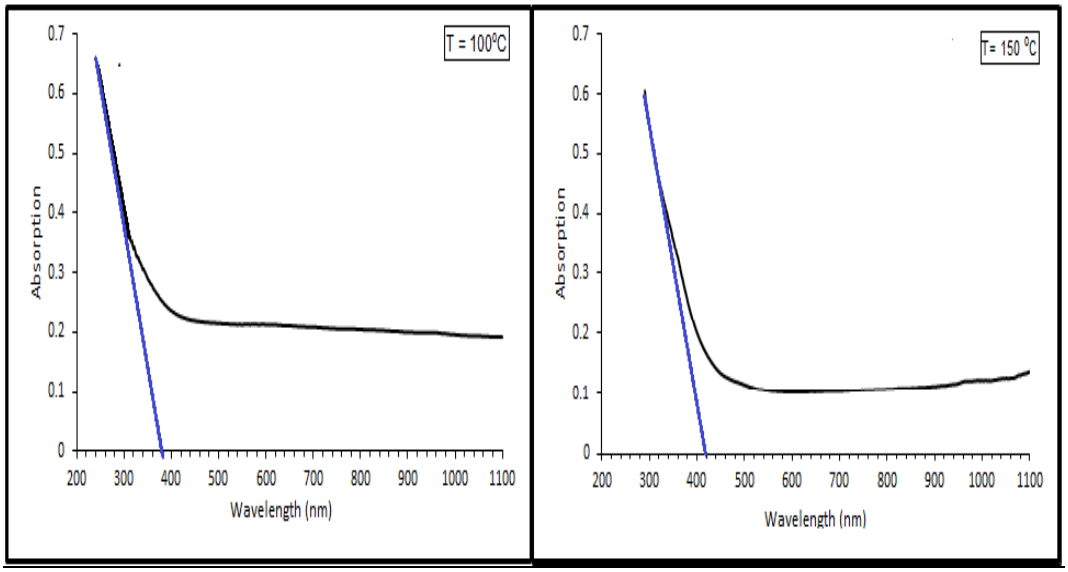

Figure 6: UV-Vis absorbance spectra of Fe_3O_4 NPs at both annealing temperatures.

The optical transmittance of prepared materials is of tremendous interest because of its scientific significance. The crystalline structure of the produced materials, as well as the surface topography, influence the optical transmittance spectra. Figure (7) shows transmission vs wavelength graphs of Fe_3O_4 NPs prepared using the green method at both annealing temperatures. Below 400 nm, the transmittance of the materials drops sharply, owing to the high absorbance of the materials in this region, while the structure becomes more transparent in the long wavelength range. Heat treatment also affects spectral characterization. The annealing process improves the optical transmittance of manufactured materials, which means less reflection and absorption. This increase could be attributed to defect reduction. Furthermore, as indicated in the XRD results, annealing improves the structure by increasing the degree of crystallization of the material structure by increasing crystal size.

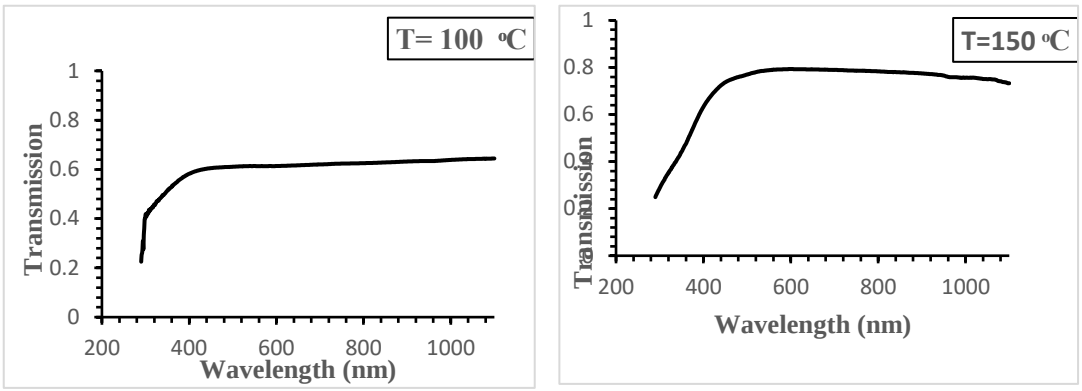

Figure 7: UV-Vis transmission spectra of Fe_3O_4 NPs at both annealing temperatures.

4. Conclusions

This study demonstrates the successful synthesis of iron oxide nanoparticles by a green approach utilizing the extract derived from Phoenix dactylifera. The X-ray diffraction patterns revealed that the Fe_3O_4 nanoparticles have a cubic structure, with the crystal size increasing as the annealing temperature was increased, as well as the formation of new peaks at 150°C that were not present at 100°C. The average grain size of the prepared nanoparticles increased from 61.80 to 87. 17 nm with the increase of the annealing temperature from 100 to 150 ^{o} C, respectively. From FE-SEM, it was observed that the particles came close to each other when the temperature increased and clumped to take an almost spherical structure. Finally, the band gap energy decreased from 3.26 to 2.95nm with increasing the annealing temperature from 100 to 150 ^{o} C, respectively.

Acknowledged

I extend my thanks to the Nanotechnology Laboratory at the College of Women's Sciences - University of Baghdad.

Conflict of Interest: The authors declare that they have no conflicts of interest.

References

[1] S. P. Council, "Nanotechnology White Paper," no. February, 2007.

[2] Z. J. Shanan, M. D. Majed, and H. M. J. Ali, "Effect of the concentration of Copper on the properties of Copper Sulfide nanostructure," *Baghdad Sci. J.*, vol. 19, no. 1, pp. 225–232, 2022, doi: 10.21123/BSJ.2022.19.1.0225.

[3] B. Nigam, S. Mittal, A. Prakash, S. Satsangi, P. K. Mahto, and B. P. Swain, "Synthesis and Characterization of Fe3O4 Nanoparticles for Nanofluid Applications-A Review," *IOP Conf. Ser. Mater. Sci. Eng.*, vol. 377, no. 1, p. 012187, 2018, doi: 10.1088/1757-899X/377/1/012187.

[4] K. N. Thakkar, S. S. Mhatre, and R. Y. Parikh, "Biological synthesis of metallic nanoparticles," *Nanomedicine: Nanotechnology, Biol. Med.*, vol. 6, no. 2, pp. 257–262, 2010, doi: 10.1016/j.nano.2009.07.002.

[5] V. Archana, J. Joseph Prince, and S. Kalainathan, "Simple One-Step Leaf Extract-Assisted Preparation of α -Fe2O3Nanoparticles, Physicochemical Properties, and Its Sunlight-Driven Photocatalytic Activity on Methylene Blue Dye Degradation," *J. Nanomater.*, vol. 2021, pp.1-25, 2021, doi: 10.1155/2021/8570351.

[6] P. Kuppusamy, M. M. Yusoff, G. P. Maniam, and N. Govindan, "Biosynthesis of metallic nanoparticles using plant derivatives and their new avenues in pharmacological applications – An updated report," *Saudi Pharm. J.*, vol. 24, no. 4, pp. 473–484, 2016, doi: 10.1016/j.jsps.2014.11.013.

[7] A. K. Mittal, Y. Chisti, and U. C. Banerjee, "Synthesis of metallic nanoparticles using plant extracts," *Biotechnol. Adv.*, vol. 31, no. 2, pp. 346–356, 2013, doi: 10.1016/j.biotechadv.2013.01.003.

[8] A. Zelenakova, V. Zelenak, S. Michalik, J. Kovac, and M. W. Meisel, "Structural and Magnetic Properties of CoO-Pt core-shell nanoparticles," *Phys. Rev. B*, vol. 89, p. 104417, 2014, doi: 10.1103/PhysRevB.89.104417.

[9] Marin Tadic, M. Panjan, V. Damnjanovic, and I. Milosevic, "Magnetic properties of hematite (α-Fe_2O_3) nanoparticles prepared by hydrothermal synthesis method," *Appl. Surf. Sci.*, vol. 320, pp. 183–187, 2014, doi: 10.1016/j.apsusc.2014.08.193.

[10] N. Shah, I. Khan, H. Ahmad, S. S. Shah, D. Shah, S. Ahmad, and I. Khan, "Synthesis and Characterization of Starch Coated Natural Magnetic Iron Oxide Nanoparticles for the Removal of Methyl Orange Dye from Water," *Lett. Appl. NanoBioScience*, vol. 10, no. 4, pp. 2750–2759, 2021, doi: 10.33263/lianbs104.27502759.

[11] N. Kumar, A. Gaur, and R. K. Kotnala, "Stable Fe deficient Sr2Fe1-δMoO 6 ($0.0 \leq \delta \leq 0.10$) compound," *J. Alloys Compd.*, vol. 601, pp. 245–250, 2014, doi: 10.1016/j.jallcom.2014.02.173.

[12] M. Muhajir, P. Puspitasari, and J. A. Razak, "Synthesis and Applications of Hematite α-Fe2O3 : a Review," *J. Mech. Eng. Sci. Technol*., vol. 3, no. 2, pp. 51–58, 2019, doi: 10.17977/um016v3i22019p051.

[13] B. K. Pandey, A. K. Shahi, J. Shah, R. K. Kotnala, and R. Gopal, "Optical and magnetic properties of Fe 2 O 3 nanoparticles synthesized by laser ablation/fragmentation technique in different liquid media," *Appl. Surf. Sci*., vol. 289, pp. 462–471, 2014, doi: 10.1016/j.apsusc.2013.11.009.

[14] M. Valášková, J. Tokarský, J. Pavlovský, T. Prostějovský, and K. Kočí, "α-Fe2O3 nanoparticles/vermiculite clay material: Structural, optical and photocatalytic properties," *Materials (Basel)*, vol. 12, no. 11, p. 1880, 2019, doi: 10.3390/ma12111880.

[15] M. D. Nguyen , H.-V. Tran , Sh. Xu and T. R. Lee, "Fe_3O_4 Nanoparticles : Structures , Synthesis , Magnetic Properties , Surface Functionalization , and Emerging Applications," *Appl. Sci*., vol. 11, no. 23, p. 11301, 2021.

[16] R. Ali, Z. J. Shanan, G. M. Saleh, och Q. Abass, "Green synthesis and the study of some physical properties of MgO nanoparticles and their antibacterial activity," *Iraqi J. Sci.*, vol. 61, no. 2, pp. 266–276, 2020, doi: 10.24996/ijs.2020.61.2.9.

[17] Mazhir, S. N., Ali, A. H., Abdalameer, N. K., & Qasim, S. A. (2022). ZnO: Fe3O4 Nanoparticles Produced by Cold Plasma: Synthesis, Characterization and Anti-Microbial Activity. International Journal of Nanoscience, 21(03), 2250021.

[18] H. H. Murbat, N. kh. Abdalameer, A. K. Brrd and F. Abdulameer, "Effects of Non-Thermal Argon Plasma Produced at Atmospheric Pressure on the Optical Properties of CdO Thin Films Abstract," *Baghdad Sci. J*., vol. 15, no. 2, pp. 221–226, 2018.

[19] Z. J. Shanan, J. Ali, and k. A. Adem., "Structural, Morphological and Optical Properties of ZnS Thin Film Deposited by Pulsed Laser Deposition Technique," *Aust. J. Basic Appl. Sci.*, vol. 8, no 17, pp. 311–316, 2014.

[20] B. Nigam, S. Mittal, A. Prakash, S. Satsangi, P. K. Mahto, and B. P. Swain, "Synthesis and Characterization of Fe3O4 Nanoparticles for Nanofluid Applications-A Review," *IOP Conf. Ser. Mater. Sci. Eng*., vol. 377, no 1, p. 012187, 2018, doi: 10.1088/1757-899X/377/1/012187.

[21] F. Muhammad, N. N. Hussein, och G. M. Sulaiman, "Potentials of Iron Oxide Nanoparticles (Fe_3O_4): As Antioxidant and Alternative Therapeutic Agent Against Common Multidrug-Resistant Microbial Species," *Iraqi J. Sci*., vol. 64, no. 6, pp. 2759–2773, 2023, doi: 10.24996/ijs.2023.64.6.10.